Growth, Disorder and Physical Properties of ZnSnN$_2$

N. Feldberg[1], J.D. Aldous[1], W.M. Linhart[2], L. J. Phillips[2], K. Durose[2], P.A. Stampe[3], R.J.

Kennedy[3], D.O. Scanlon[4], G. Vardar[5], R.L. Field III[5], T.Y. Jen[5], R. Goldman[5], T.D. Veal[2], and

S.M. Durbin[1, 6]

[1]Department of Physics, University at Buffalo, Buffalo, NY 14260, USA

[2]Stephenson Institute for Renewable Energy and Department of Physics,

University of Liverpool, Liverpool, UK

[3]Department of Physics, Florida A&M University, Tallahassee, FL, USA

[4]University College London, Kathleen Lonsdale Materials Chemistry, Department of

Chemistry, 20 Gordon Street, London WC1H 0AJ, United Kingdom

[5]Department of Materials Science and Engineering, University of Michigan, Ann Arbor

USA

[6]Department of Electrical Engineering, University at Buffalo, Buffalo, NY 14260, USA

Abstract

We examine ZnSnN$_2$, a member of the class of materials contemporarily termed "earth-abundant

element semiconductors," with an emphasis on evaluating its suitability for photovoltaic

applications. It is predicted to crystallize in an orthorhombic lattice with an energy gap of 2 eV.

Instead, using molecular beam epitaxy to deposit high-purity, single crystal as well as highly

textured polycrystalline thin films, only a monoclinic structure is observed experimentally. Far

from being detrimental, we demonstrate that the cation sublattice disorder which inhibits the

orthorhombic lattice has a profound effect on the energy gap, obviating the need for alloying to match the solar spectrum.

Significant volatility in the price and supply of indium and gallium over the past decade has led to considerable concern given their critical roles in a wide range of electronic devices.[1] It also has nontrivial implications for photovoltaic materials set to compete with silicon, given that market's particular emphasis on low cost, low toxicity manufacturing. An interesting potential alternative family was proposed recently by Punya et al., who noted that the band gaps of ternary heterovalent compounds formed with nitrogen in conjunction with equal amounts of column II and column IV metals should span the visible spectrum.[2] Closely related to the chalcopyrite family of II-IV-$(P,As)_2$ materials proposed by Goodman in 1957,[3] they are to the III-nitride family what $CuInSe_2$ is to $ZnSe$. However, outside of limited interest for their nonlinear optical properties, these unusual semiconductors have been largely ignored.

Two members of this family, at least, now warrant renewed attention. $ZnSiN_2$ and $ZnSnN_2$ represent analogs to AlN and InN respectively, and are comprised solely of so-called "earth-abundant" elements. The crustal abundance of indium is approximately 0.25 ppm, only three times that of silver; the occurrence of gallium is only slightly greater.[1,4] In contrast, the occurrence of tin is two orders of magnitude greater than that of indium, and that of zinc is three orders of magnitude greater.[5,6] Moreover, recycling infrastructure for Zn, Sn and Si already exists, with roughly one third of the annual US supply of Zn and Sn originating directly from reclamation sources.[5,6] Consequently, these materials are attractive not only for economic reasons, but from an environmental perspective as well.

There are a number of reports in the literature describing the synthesis and preliminary characterization of both $ZnSiN_2$[7-9] and the closely related material $ZnGeN_2$,[8-15] the two largest band gap energy (approximately 5.5 eV and 3.5eV, respectively[2]) members of this semiconductor family. Very little appears in the literature regarding $ZnSnN_2$ however, and it is only in the last year that the first reports of its synthesis have surfaced.[16,17] First-principles calculations suggest a band gap energy of approximately 2.0 eV.[2,17] Recently, Lahourcade et al. have described measurements of the optical gap of sputter-deposited polycrystalline thin films reported to have the orthorhombic structure, and compared them to predictions from first-principles calculations.[16] They observe a measured absorption onset of approximately 1.8 eV, which differs somewhat from their own predicted bandgap value of 1.42 eV. This is explained by the presence of a Burstein-Moss shift, but is seemingly inconsistent with the band gap put forward independently by Punya et al. and Feldberg et al. of about 2 eV for the orthorhombic structure.[2, 17]

In this letter, we demonstrate that such films are more likely monoclinic, a situation which results from disorder in the cation sublattice. The corresponding variation in lattice periodicity has profound consequences for the energy gap of the material. However, in contrast to being detrimental, controlled amounts of disorder in the cation sublattice, along the lines proposed first by Jaffe and Zunger[18] and recently revisited by Walsh and Scanlon,[19] are potentially of practical benefit. It may in fact provide a pathway to physically tailoring the electronic properties of this material, potentially eliminating the need for alloying to achieve a desired band gap energy.

Single-crystal thin films of $ZnSnN_2$ were obtained utilizing a modified Perkin Elmer 430 molecular beam epitaxy (MBE) system. Conventional effusion cells were employed for evaporation of Zn and Sn, with atomic fluxes measured by a moveable quartz crystal

microbalance placed in close proximity to the substrate position. Active nitrogen was supplied using an Oxford HD25 inductively coupled RF plasma source equipped with a 488 hole aperture plate and electrostatic ion removal. Films were grown on (111) YSZ substrates which were first subjected to a standard three-step solvent cleaning sequence consisting of trichloroethane, acetone and methanol. Samples were examined in-situ using a 20 kV Staib Instruments reflection high-energy electron diffraction (RHEED) system in conjunction with a KSA 400 image acquisition and analysis package, and ex-situ using x-ray diffraction, Rutherford backscattering spectrometry (RBS), and electron microscopy. Near-infrared and visible reflectance and transmittance measurements at an incident angle of 11° relative to the surface normal were performed at room temperature using a Bruker Vertex 70V Fourier-transform infrared/visible (FTIR) spectrometer using a tungsten lamp, a Si diode detector and a quartz beamsplitter. The transmittance and reflectance spectra were used to calculate the absorption coefficient. Hall effect measurements were performed between 25 and 300 K in the Van der Pauw configuration with a 0.8 T magnetic field.

Experimental results were compared to detailed calculations performed using the periodic density functional theory (DFT) code VASP,[20, 21] in which a plane-wave basis set describes the valence electronic states. The Perdew-Burke-Ernzerhof (PBE) gradient corrected functional was used to treat the exchange and correlation.[22] The projector-augmented wave (PAW) method was used to describe the interactions between the cores (Zn:[Ar], Sn:[Kr] and N:[He]) and the valence electrons,[23, 24] so that the Zn $3d$ and Sn $4d$ states were explicitly included. In this study we have employed the hybrid density functional developed by Adome and Barone (PBE0) [25] as implemented in the VASP code.[26] In the PBE0 approach, a value of exact non-local exchange, α, of 25% is added to the PBE formalism. The PBE0 approach has been shown to slightly

overestimate the band gaps of III-V materials [27] but is considered a better choice than the HSE06 functional, which needs the percentage of exchange α to be increased to an empirical 30-35% to yield good agreement with experimental data. [28]

The very disparate vapor pressures of Zn and Sn present a significant challenge in growing stoichiometric $ZnSnN_2$ thin films, and initial attempts yielded Sn-rich polycrystalline samples as revealed by RBS until the appropriate Zn:Sn atomic flux ratio was determined (approximately 20:1, at a substrate temperature of 400°C and near-unity nitrogen to total effective metal flux conditions). At this temperature little if any excess (unreacted) Sn was able to desorb, whereas significant desorption of Zn was observed as evidenced by Sn-rich metal coverage on initial films. Subsequently, films grown under appropriate Zn-rich conditions were single crystal as determined by in-situ RHEED, although still Sn rich (Sn:Zn ratio of 1.2:1). No metal coverage was evident for the single-crystal films, which had a slight orange coloration visible to the naked eye.

Regardless of crystallinity, all films were found to exhibit the monoclinic lattice structure as determined by x-ray diffraction, as opposed to the expected equilibrium orthorhombic structure. P36 and P50 are representative samples of the single crystal films which were obtained. Figure 1(a) shows a θ-2θ figure representative of the single crystal films exhibiting monoclinic symmetry. The lack of orthorhombic structure is evident by the conspicuous absence of 0kk reflections in pole figures measured at a 2θ angle of 22° (Fig. 1(b)): lattice calculations show this peak should have at least 20% of the intensity of the 004 reflections. Even slow scans with long averaging times showed no detectable reflections at this angle. Lattice parameters were obtained from single crystal fitting of a minimum of twenty lattice reflections; fitted lattice parameters for two representative single crystal films (P36 and P50) are provided in Table 1. The orthorhombic
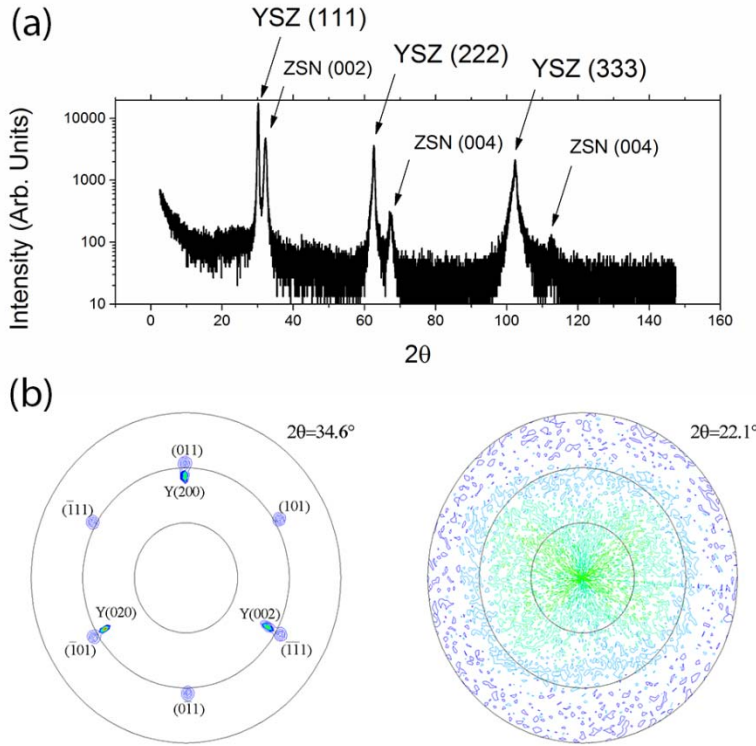
Figure 1: (a) θ/2θ measurements show only 002, 004, and 006 ZnSnN₂ and 111, 222, and 333 YSZ substrate reflections. (b) Pole figure measured at 2θ = 34.6° shows the (200) peaks of the YSZ substrate, as well as the 0kk reflections of the monoclinic ZnSnN₂. Pole figure at 22.1° shows no evidence of a diffraction peak.

lattice parameters are calculated by assuming all observed reflections to be due to an orthorhombic lattice (ignoring the absent reflections) and are listed only for comparison purposes. The monoclinic lattice can be understood as resulting directly from disorder in the cation sublattice. This changes the unit cell as illustrated in Fig. 2, where even partial randomization of Zn and Sn atoms on cation lattice sites alters the symmetry. Consequently, care must be taken in identifying the structure using x-ray diffraction. We note that Atwater et al. drew different conclusions regarding the structure of their thin films, where they favored the orthorhombic $Pna2_1$ structure based on the width of their observed peaks due to peak splitting

compared with what is expected for the wurtzite structure. Their figure of the expected peaks for the orthorhombic Pna2$_1$ structure also contained a peak of significant intensity at 22°, but, just as in our case, it was not observed experimentally.

Table 1 Fitted lattice parameters assuming either orthorhombic or monoclinic lattices for two representative films, together with the calculated lattice parameters.

Lattice	a (Å)	b (Å)	c (Å)	α(°)	β (°)	γ (°)
P36 Monoclinic	3.375(1)	3.376(1)	5.532(3)	89.98(4)	89.99(4)	119.93(3)
P36 Orthorhombic	6.752(4)	5.850(3)	5.533(4)	89.98(5)	90.04(5)	90.07(5)
P50 Monoclinic	3.383(4)	3.379(3)	5.567(6)	89.97(9)	89.96(9)	119.95(7)
P50 Orthorhombic	6.766(7)	5.855(5)	5.568(9)	89.95(9)	89.96(7)	89.9(1)
PBE0 Monoclinic	3.392	3.412	5.416	89.93	89.96	120.16
PBE0 Orthorhombic	6.755	5.846	5.473	90.00	90.00	90.00

The somewhat hotly debated revision of the band gap of InN from ~2 eV to ~0.7 eV[29] suggests that conclusions about the optical properties of ZnSnN$_2$ should not be drawn too readily or conclusively. With this in mind, in addition to growth and structural properties, the optical and transport properties of the MBE-grown ZnSnN$_2$ films have also been investigated. Variable temperature Hall effect measurements on the two 125 nm-thick single-crystal ZnSnN$_2$ films of Table 1 reveal that both are degenerately n-type – the carrier density does not vary with

temperature. Sample P36 has a free electron density $n = 1.1 \times 10^{21}$ cm^{-3} and a mobility $\mu = 10$ cm^2/Vs; sample B has $n = 3 \times 10^{20}$ cm^{-3} and $\mu = 10$ cm^2/Vs.
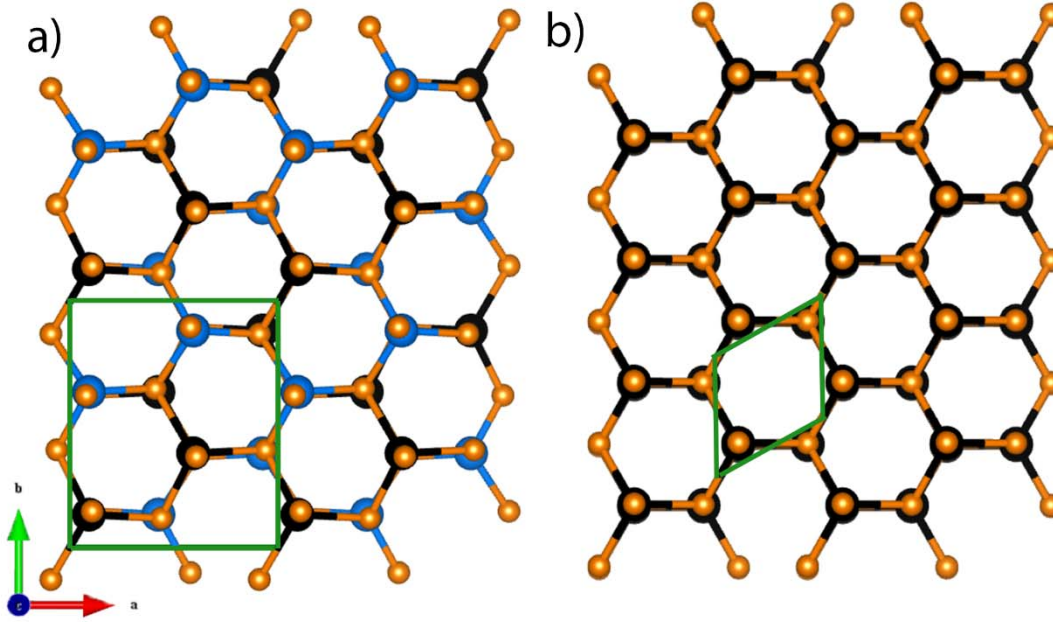

Figure 2: (color online) Possible lattice structures of ZnSnN$_2$: (a) Orthorhombic (ordered cation sublattice); Zn and Sn are represented by distinct colors (b) Monoclinic (disordered cation sublattice) with γ near 120°; Zn and Sn are random and represented by the same color. In both images the smallest atoms represent nitrogen. Unit cells are outlined.

The optical absorption spectra from these two single crystal ZnSnN$_2$ films are shown in Fig. 3. The absorption onsets are at 2.12 eV for sample P36 and 2.38 eV for sample P50, respectively. The absorption coefficient α rapidly increases to 5×10^4 cm^{-1} above each onset, a value typical of direct band gap semiconductors. The plot of α^2 versus photon energy exhibits approximately linear behavior, again consistent with – but not proof of – a direct band gap. The below onset feature for both spectra is due to Fabry-Perot oscillations associated with the 125 nm ZnSnN$_2$ film thickness. The evidence of unintentional degenerate n-type doping from Hall effect indicates that the absorption spectra are influenced by conduction band filling, the well-known

Burstein-Moss shift[30, 31]. That is, optical absorption is forbidden for transitions below the Fermi level; only direct transitions from the valence band to the states at or above the Fermi level contribute to the absorption spectra. Considering a Burstein-Moss shift alone, sample P36, with the higher free electron density, would be expected to have the higher absorption edge. However, we find that sample P50 with the lower electron concentration has the highest energy absorption onset.
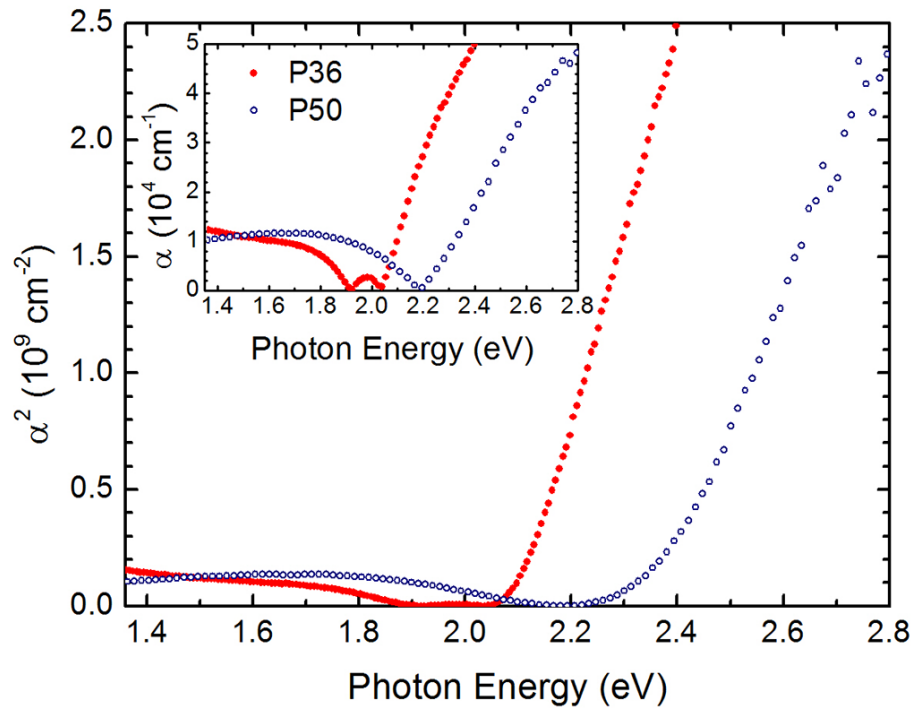

Figure 3: Optical absorption spectra from two 125 nm-thick ZnSnN$_2$ films; samples P36 and P50 grown under identical conditions except for the nitrogen flux being halved.

To investigate the potential effects of cation sublattice disorder on electronic properties, DFT was employed using a 72 atom supercell with cation placement based on the special quasi-random structure (SQS) approach, [32] and k-point sampling of Γ centered $2\times2\times2$. Calculations were deemed to be converged when the forces on all the atoms were less than 0.01 eV Å^{-1}.In the case of the perfectly ordered orthorhombic lattice with Pna2$_1$ space group, our PBE0 calculations

yield a band gap (at zero Kelvin) of 2.09 eV, in excellent agreement with the quasiparticle self-consistent GW approximation result of Punya et al.[2] In contrast, the calculated band gap for disordered monoclinic $ZnSnN_2$ is 1.12 eV, fully 0.97 eV narrower than the ideally ordered orthorhombic structure, as illustrated in Fig. 4.
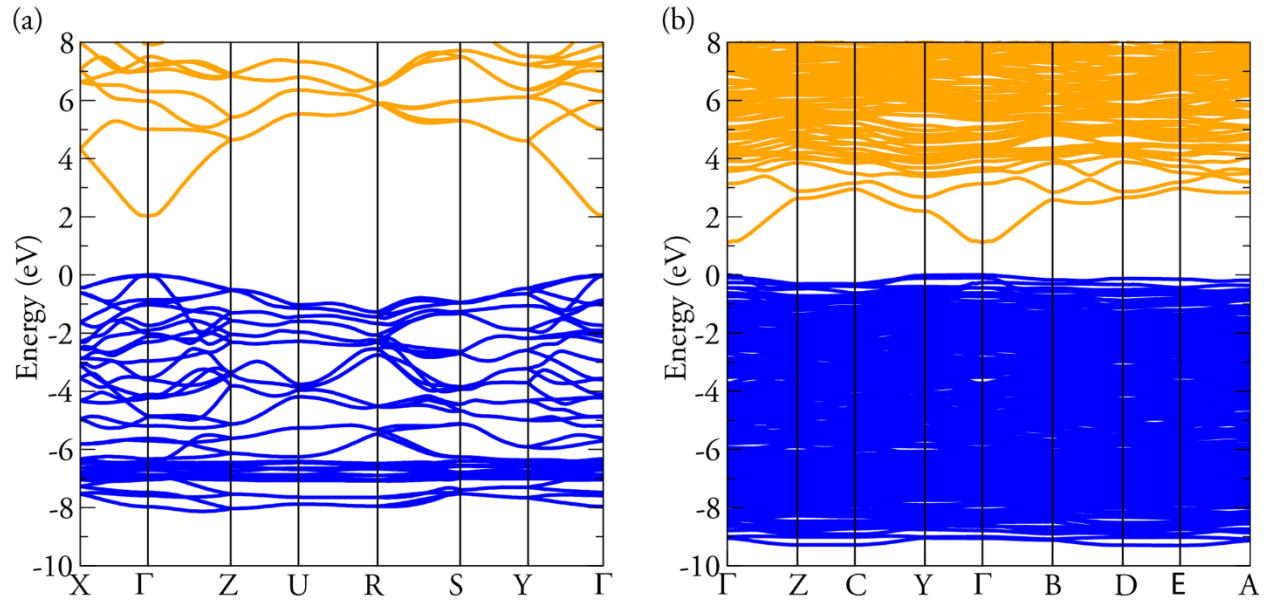

Figure 4: Calculated band structure for (a) orthorhombic lattice and (b) monoclinic lattice with fully disordered cation sublattice.

The PBE0 calculated fully disordered monoclinic structure was found to be metastable with an increase in energy of 0.089 eV per atom compared to the orthorhombic phase. The optical absorption and Hall effect results shown above may, therefore, represent a complicated interplay between Burstein-Moss shift due to conduction band filling and changes of the fundamental gap associated with different degrees of cation disorder. Accordingly, sample P36 is suggested to have the greater cation disorder and the lower fundamental band gap, while sample P50 has less cation disorder and the higher fundamental band gap. Samples P36 and P50 were grown under identical conditions except that sample P50 was grown with half the nitrogen flux of sample P36,

making its growth conditions more metal-rich. Such conditions are known to produce improved quality III-nitride thin films[33,34] consistent with the lower carrier density of sample P50, and the suggestion that it may have greater cation ordering.

A direct consequence of this is the intriguing possibility of tuning the band gap energy through controlled disorder of the cation sublattice (introduced, for example, by adjusting growth conditions such as substrate temperature and metal/nitrogen flux ratio). Such behavior has the potential to obviate the need for alloying to adjust the band gap to match the solar spectrum. In fact, such behavior is not unique to the $Zn-IV-N_2$ system. Scanlon and Walsh pointed out that $ZnSnP_2$ experiences a similar bandgap narrowing with cation disordering[19]. The degree of ordering is expected to vary continuously and leads to a continuum of bandgap values. Additional examples of ordering-based energy gap adjustment include $GaInP_2$, where a much smaller (~135 meV) range of values is achievable.[35] A key issue is the quantification of disorder which has been attempted for the wider bandgap $ZnGeN_2$. Using neutron scattering on $ZnGeN_2$ it was confirmed that disorder in this closely related material does in fact result in monoclinic as opposed to orthorhombic structure, which supports the present conclusions.[15]

In conclusion, single-crystal thin films of $ZnSnN_2$ have been obtained using a plasma-assisted molecular beam epitaxy process. Regardless of film quality, all samples exhibited the monoclinic lattice structure in contrast to the predicted orthorhombic lattice structure and the report of Lahourcade et al. This is attributed to a partially disordered cation sublattice, which calculations show can reduce the electronic band gap by as much as 0.95 eV, opening the possibility for band gap engineering through intentional introduction of controlled amounts of disorder.

Acknowledgements

1.   A. C. Tolcin, in *Mineral Commodity Summaries 2013* (U.S. Geological Survey, Reston, Virginia, 2013), pp. 74-76.

2.   A. Punya, W. R. L. Lambrecht and M. van Schilfgaarde, Phys. Rev. B **84**, 165204 (2011).

3.   C. H. L. Goodman, Nature **179**, 828 (1957).

4.   B. W. Jaskula, in *Mineral Commodity Summaries 2013* (U.S. Geological Survey, Reston, Virginia, 2013), pp. 58-60.

5.   A. C. Tolcin, in *Mineral Commodity Summaries 2013* (U.S. Geological Survey, Reston, Virginia, 2013), pp. 188-189.

6.   J. F. Carlin, in *Mineral Commodity Summaries 2013* (U.S. Geological Survey, Reston, Virginia, 2013), pp. 170-171.

7.   T. Cloitre, A. Sere and R. L. Aulombard, Superlattice Microst **36**, 377 (2004).

8.   T. Endo, Y. Sato, H. Takizawa and M. Shimada, J Mater Sci Lett **11**, 424 (1992).

9.   J. Muth, A. Cai, A. Osinsky, H. Everitt, B. Cook and I. Avrutsky, MRS Online Proceedings Library **831** (2004).

10.   K. Du, C. Bekele, C. C. Hayman, J. C. Angus, P. Pirouz and K. Kash, J Cryst Growth **310**, 1057 (2008).

11.   M. Maunaye and J. Lang, Mater Res Bull **5**, 793 (1970).

12.   T. Misaki, K. Tsuchiya, D. Sakai, A. Wakahara, H. Okada, A. Yoshida, Phys Status Solidi C **0**, 188 (2002).

13.   J. E. Van Nostrand, J. D. Albrecht, R. Cortez, K. D. Leedy, B. Johnson and M. J. O'Keefe, J. Electron Mater **34**, 1349 (2005).

14.   R. Viennois, T. Taliercio, V. Potin, A. Errebbahi, B. Gil, S. Charar, A. Haidoux and J. C. Tédenac, Mater Scie Engin-B **82**, 45 (2001).

15.   M. Wintenberger, M. Maunaye and Y. Laurent, Mater Res Bull **8**, 1049 (1973).

16.   L. Lahourcade, N. C. Coronel, K. T. Delaney, S. K. Shukla, N. A. Spaldin and H. A. Atwater, Adv Mater **25**, 2562 (2013).

17.   N. Feldberg, B. Keen, J. D. Aldous, D. O. Scanlon, P. A. Stampe, R. J. Kennedy, R. J. Reeves, T. D. Veal and S. M. Durbin, Proc. of the 38th IEEE Photovoltaic Specialists Conference (PVSC), 002527 (2012).

18.   J. E. Jaffe and A. Zunger, Phys Rev B **27**, 5176 (1983).

19.   D. O. Scanlon and A. Walsh, Appl Phys Lett **100**, 251911 (2012).

20.   G. Kresse and J. Furthmüller, Phys Rev B **54**, 11169 (1996).

21.   G. Kresse and J. Hafner, Phys Rev B **49**, 14251 (1994).

22.   J. P. Perdew, K. Burke and M. Ernzerhof, Phys Rev Lett **77**, 3865 (1996).

23.   P. E. Blöchl, Phys Rev B **50**, 17953 (1994).

24.   G. Kresse and D. Joubert, Phys Rev B **59**, 1758 (1999).

25.   C. Adamo and V. Barone, The Journal of Chemical Physics **110** (13), 6158-6170 (1999).

26.   J. Paier, M. Marsman, K. Hummer, G. Kresse, I. C. Gerber and J. G. Angyan, J Chem Phys **124**, 154709 (2006).

27.   X. Wu, E. J. Walter, A. M. Rappe, R. Car and A. Selloni, Phys Rev B **80**, 115201 (2009).

28.   P. G. Moses, M. Miao, Q. Yan and C. G. V. d. Walle, J Chem Phys **134**, 084703 (2011).

29.   V.Yu Davydov and A.A. Klochikhin, *Indium Nitride and Related Alloys,* T. D. Veal, C. F. McConville and W. J. Schaff, eds. (CRC Press, Boca Raton, Fl, 2010), 181-242.

30.   E. Burstein, Phys Rev **93**, 632 (1954).

31.   T. S. Moss, Proc Phys Soc London Sect B **67**, 775 (1954).

32.   A. Zunger, S. H. Wei, L. G. Ferreira and J. E. Bernard, Phys Rev Lett **65**, 353 (1990).

33.   A.R. Smith, R.M. Feebstra, D.W. Greve, M.-S. Shin, M. Skowronski, J. Neugebauer, J.E. Northrup, J Vac Sci Tech B **16**, 2242 (1998).

34.   G. Koblmüller, J. Brown, R. Averbeck, H. Riechert, P. Pongratz and J. S. Speck, Japan J Appl Phys **44**, L906 (2005).

35.   J. K. Shurtleff, R. T. Lee, C. M. Fetzer and G. B. Stringfellow, Appl Phys Lett **75**, 1914 (1999).

(a)

YSZ (111)

ZSN (002)

YSZ (222)

ZSN (004)

YSZ (333)

ZSN (004)

Intensity (Arb. Units)

2θ

(b)

2θ=34.6°

(011)

Y(200)

(̄111)

(101)

Y(020)

Y(002)

(101)

(̄111)

(011)

2θ=22.1°